This is a peer-reviewed, accepted author manuscript of the following research article: Aitchison, C. M., & Sprick, R. S. (2021). Conjugated nanomaterials for solar fuel production. *Nanoscale*, *13*(2), 634-646. https://doi.org/10.1039/d0nr07533g

Conjugated nanomaterials for solar fuel production

Catherine M. Aitchison,[a] Reiner Sebastian Sprick,[b,*]

Received 00th January 20xx,
Accepted 00th January 20xx

DOI: 10.1039/x0xx00000x

Photocatalytic hydrogen production from water has the potential to fullfill future energy needs by producing a clean and storable fuel. In recent years polymer photocatalysts have attracted significant interest in an attempt to address these challenges. One reason organic photocatalysts have been considered an attrative target is their synthetic modularity, therefore, the ability to tune their opto-electronic properties by incoorporating different building blocks. A wide range of factors has been investigated and in particular nano-sized particles have found to be highly efficient due to a size effect resulting from the ability of these to increase the number of charges reaching catalytic sites.

Introduction

The rising energy demand of our societies has resulted in the emission of large amounts of carbon dioxide, which has been the main driver of climate change. Solar energy has the potential to fulfil global energy needs[1] but the temporal and spatial inconsistency of this supply, as well as the need for energy to be used in non-grid applications, pose significant challenges. For this reason, there has been much focus on developing batteries that can store the electricity generated from photovoltaics, but an alternative approach is to store solar energy as chemical fuel. This can be achieved by coupling photovoltaics with electrolysers that produce hydrogen from water. Hydrogen can then be used in fuel cells to generate electricity or used directly in industrial processes. Hydrogen can also be produced in one-step from solar energy via photoelectrochemical[2] or photocatalytic[3–5] water splitting. The latter of these has the advantage of being technologically simple, with lower projected scale-up costs.[6]

In photocatalytic water splitting a semiconductor is dispersed in water under light irradiation and facilitates the coupled redox reactions of proton reduction and water oxidation. Although materials are often first studied for one or other of the half reactions in the presence of a scavenger. Most of the semiconductors studied to date are inorganic and systems such as lanthanum-doped $SrTiO_3$[7] have been reported with very high efficiencies, in particular under UV irradiation.[8] Carbon nitride was first reported to be photocatalytically active for proton reduction in 2009[9] and was amongst the first examples of 'soft' material for this purpose, i.e. one that contains only light elements. Whilst the idealised structure (C_3N_4) contains no C-H bonds it is still usually classified as an organic semiconductor, as experimental samples generally contain significant amounts of hydrogen. In recent years, a range of other organic polymer photocatalysts, such as linear conjugated polymers,[10–19] conjugated polymer networks,[20–24] covalent organic frameworks,[25,26] oligomers[27–29] and molecular crystals,[30] have been reported to be active for hydrogen production, as well as for a variety of other light-driven transformations.[31]

The interest in these materials is a consequence of the fact that they are synthetically modular with a large range of building blocks available and that they are made at low temperatures. This results in materials with a defined molecular structure or repeat unit, potentially giving control over many factors that are important to photocatalytic water splitting.

Performance determining factors for organic photocatalysts

Factors that influence photocatalytic activity

Light absorption, in particular the ability of the semiconductor to absorb in the visible light range and ideally in the near infra-red region, is an important factor to match the available solar light at ground level. As well as absorbing across a wide range of wavelengths a good photocatalyst will also have a large magnitude of absorption *i.e.* a high extinction coefficient. Combined, these two factors determine the proportion of incident radiation that could be used by a particular photocatalyst. An energy gap of 1.23 V is required to drive water splitting; however, it is also crucial that the position of the of the HOMO and the LUMO allow for an overpotential that is sufficient to overcome any kinetic barriers associated with proton reduction or water/hole scavenger oxidation. (Figure 1a). When a photon with energy greater than the band-gap of the semiconductor is absorbed excited state species are generated. In organic materials these are usually strongly bound Frenkel-type excitons[32] and significant losses can occur due to recombination or other internal conversion processes before separation of such excitons into charge carriers. Separation can occur when excitons diffuse to the surface of the material and undergo electron transfer to/from

[a] *Department of Chemistry, Chemistry Research Laboratory, University of Oxford, Oxford, OX1 3TA UK.*
[b] *Department of Pure and Applied Chemistry, University of Strathclyde, Thomas Graham Building, 295 Cathedral Street, Glasgow G1 1XL, Scotland, UK. Email: Sebastian.Sprick@strath.ac.uk*

a scavenger molecule[12,33] or a metal cocatalyst.[13] Alternatively, excitons can separate at donor-acceptor interfaces, where charge transfer between HOMOs or LUMOs with offset energies can be sufficient to overcome exciton binding energies. The charge carriers, normally described as electron polarons and hole polarons in polymeric materials, are then transferred to active sites and result in hydrogen production and water/ hole scavenger oxidation respectively or are lost in further recombination processes.

Strategies for improving photocatalytic activity

Light absorption of polymer photocatalysts can be tuned using a wide range of building blocks and dyes, building on the expertise that exists in making materials for organic photovoltaic cells, although with the added complication of positioning the HOMO and LUMO levels so as to have sufficient driving forces for both half reactions. A higher degree of order within materials seems to improve their photocatalytic activity as a lower density of defects might reduce exciton recombination events and improves the transport of excitons to the interface. It is also important to consider the wettability of the polymer photocatalyst surface. Organic semiconductors are typically far less polar than inorganic photocatalysts, such as metal oxides, due to the use of large aromatic building blocks. The incorporation of polar groups, such as sulfones,[12] pyridines,[14] quaternary ammonium,[15,28] or oligo(ethylene glycol)s[16] can be used to overcome this issue and has been shown to be very efficient. The introduction of polar units also seems to improve other factors, such as charge-separation by attracting water and scavengers onto the surface of the photocatalyst.[12]

Metal cocatalysts on the surface of the materials are also thought to play an important role in polymer systems and indeed have been found to be crucial for hydrogen or oxygen production in some materials.[13,34] Metal nanoparticles or clusters are thought to lower the activation energy for charge transfer by acting as sites for charge accumulation and/or for coordination of water, scavengers or protons. Where present, residual metal from material synthesis, such as Pd or Ni particles can act as cocatalysts, but the addition of metal nanoparticles to polymers by photo- or thermal deposition is also common.

'Design' strategies for improving photocatalytic activity have yielded exciting results over the past few years but the fact that hydrogen production rate is multi-factor variable poses a significant challenge. For example, changes to chemical structure are often used to modulate a materials absorption or frontier molecular orbital energies but this will also affect an array of other material properties such as crystallinity, the degree of polymerisation or π-π stacking. Similarly processing techniques may be employed to increase crystallinity but can also affect surface texture or dispersibility. The challenge of deconvoluting the effect of individual material properties on photocatalytic activity is portrayed in Figure 1b.

Particle size and photocatalytic activity

While many studies examine one or multiple of the properties shown in Figure 1b., a factor that is often overlooked is the particle size of polymer photocatalysts. This can be tuned using a variety of processes (discussed below) but particle size of bulk materials synthesised in precipitation reactions can also vary as a secondary effect of altering synthesis conditions or monomer structure. Thus, when comparing chemically different conjugated materials' photocatalytic activity, changes in particle size have to be taken into account to rule out the possibility that this is the predominant factor. Indeed a study on fluorene-type co-polymers has shown that particle size was a dominant factor of importance for their activity, with materials that consist of large particles being less active.[22] This highlights that changes in particle size should always be considered when exploring structure–activity relationships.

The reason for an activity-size effect in polymer photocatalysts is the fact that exciton diffusion lengths are typically shorter (10s of nm) than the length scales over which light can penetrate into organic semiconductors (100s of nm).[35] In bulk materials (typically μm scale) this results in a 'dead zone' for excitons that are generated within the material at positions further away from the interface than their exciton diffusion length (Figure 2). These excitons recombine before reaching the particle surface and therefore cannot contribute to catalysis. In nanoparticles, however, excitons can only be generated at positions close to the particle surface, typically within the exciton diffusion length, meaning a higher proportion reach the surface and can drive catalysis. In order to obtain the highest photocatalytic activities, the dimension of the photocatalyst should thus be similar to the exciton diffusion lengths. This can be achieved using photocatalysts that swell in water and therefore expose more of the bulk material to water and scavenger, reducing the distance that excitons have to travel to the interface. An alternative approach is to use polymeric photocatalysts that have permanent porosity, such as conjugated microporous polymers[20] or covalent organic frameworks.[25] These materials have, in principle, a much larger interface with water and scavengers. However, water penetration into these materials does not necessarily corelate with gas-sorption-derived porosity parameters, with the pore size and the presence of hydrophilic groups also important in determining whether the pore structure is wettable. Very high photocatalytic activities have been reported for materials with wettable pore structures[25] but mass transport into and out of the material could become limiting as these materials become more efficient.[23] For this reason, nanomaterials are interesting alternative to porous polymer photocatalysts that in principle do not suffer from the same mass transport issues. Nanoparticles are also more dispersible than their bulk analogues meaning colloidally stable aqueous suspensions can be used for photocatalysis. This is particularly important for more hydrophobic polymers where bulk particles can flocculate over minutes, even when stirred, and result in suspensions that are not optically opaque.

Conjugated nanomaterials

Nanomaterials made via synthetic approaches

The most widely studied organic semiconductor for photocatalytic proton reduction is carbon nitride. It is typically synthesised by high temperature condensation of melamine, dicyandiamide or urea forming a melon-type polymer.[9] Varying the condensation temperature and heating ramp rates can dramatically alter the degree of condensation,[29] but the conditions of synthesis offer little flexibility in terms of controlling particle size or nanostructure. Precursor selection, on the other hand, can have a large effect on these properties; carbon nitrides formed from urea are the most active photocatalyst for hydrogen production[36,37] a phenomenon generally ascribed to more complete polymerisation and chemical structures closer to the idealised 2D sheets of C_3N_4.[38] However, the activity of melamine derived carbon nitrides can be improved dramatically by using a hydrogen bonded assembly of melamine and cyanuric acid as a precursor.[39] Thomas *et al*. first showed that nano- to microscale crystals of this hydrogen bond donor / acceptor pair formed from precipitation in DMSO could be condensed at high temperatures to form carbon nitrides that retained, to some extent, the microstructure of the precursor crystals.[40] Antonietti *et al*. found similar supramolecular assemblies could be formed from suspensions of the same molecules in solvents they were only slightly soluble in, such as ethanol, chloroform and water, and that the morphology of the resulting melamine/cyanuric acid assemblies varied from plate-like to rod-like to needle-like between solvents.[41] Upon condensation this resulted in carbon nitrides with a variety of different microstructures. Both groups observed the formation of hollow cavities in their materials by SEM – presumably due to the volume loss associated with NH_3 and H_2O formation during condensation. It is also worth noting that whilst SEM showed the precursor assemblies to be made up of nanoscale primary particles, these tended to aggregate into significantly larger clusters. In the precursor, the nanoscale particles may be bound by only weak Van der Waals interactions but in the corresponding carbon nitrides polymerisation fuses the primary structures irreversibly resulting in micro-scale rather than nanoscale particles sizes in suspension. These microparticles can show hydrogen evolution rates up to 7 times those of bulk carbon nitride synthesised from melamine which the authors attribute to more efficient separation and migration of charge carriers from the bulk to surface active sites in the nanostructured materials.[39] Ultimately however, it is difficult to deconvolute the effects of semiconductor morphology when comparing materials made from different chemical precursors and which contain potentially different functional groups.

An similar approach was used by Che *et al.* who 'pre-associated' melamine and glucose before thermal polymerisation to form carbon nitride nanosheets.[42] In this case the authors focus less on any preservation of crystalline nanostructure from the precursors and instead claim the route generates an in-plane heterojunction of carbon nitride adjacent to 'stitched in' areas of carbon rings. Interestingly, when loaded with a Pt cocatalyst this nanomaterial was capable of stochiometric hydrogen and oxygen from pure water with a high external quantum efficiency (EQE), of 5% at 420 nm. It is perhaps worth noting that the authors also report relatively high rates of OWS for 'standard' melamine derived carbon nitrides on their set-up, a phenomenon not usually observed without specific oxide catalysts for oxygen evolution.[43]

Carbon nanodots, carbon rich nanoparticle cores with functionalised surface carbonyl, carboxyl, hydroxylamine, amide, or sulfonic acid groups, are semiconductors and can show absorption spectra that extend into the visible region.[44] The HOMO and LUMO in these materials are dictated by the particular mixture of sp2 hybridized graphitic carbon, amorphous carbon and heteroatom dopants present in the matrix and can reside at appropriate energy levels to drive photocatalytic reactions, such as proton reduction. From a morphological point of view carbon nanodots are particularly interesting because of their very small (generally 2-10 nm) particle sizes. Aside from the obvious benefit of high extrinsic surface area, small particle sizes along with the hydrophilic surface groups means that carbon nanodots can be dispersed in water at relatively high concentration with good colloidal stability.

Carbon dots have been used as semiconductors for CO_2 reduction[45] and have also been shown to be moderately active for hydrogen production using sacrificial electron donors[46,47] and when coupled with biomass oxidation.[48] These examples use a homogenous molecular nickel (or cobalt) co-catalyst to facilitate proton reduction and, interestingly, were shown to be inactive when photodeposition of a typical Pt precursor (K_2PtCl_4) was attempted (possibly due to carboxylic acid surface groups).[46] Whilst such molecular cocatalysts are preferable to Pt / Pd heterogenous nanoparticle or cluster cocatalysts in terms of cost and the abundance of materials, they are significantly less stable and can be the limiting factor for photocatalytic longevity in these systems – rather than photosensitizer degradation. Carbon dots can be made by hydrothermal treatment of readily available precursors such as citric acid[49] and glucose,[50] or even food waste.[51] Whilst this technique is cheap and easily scalable relatively little is known about the exact chemical structures formed during these reactions. The very small length scale of carbon dots means that particle size could also affect the materials frontier molecular orbitals energies and, subsequently, the onset of absorption and overpotentials available for redox reaction. Ab initio modelling by Guldi *et al.* indicates that electronic structure is highly dependent on particle size of (particularly small 1- 2 nm) carbon nanodots as this modulates the size of sp2 conjugated domains.[52] There is also some evidence of this experimentally; Yuan *et al.* controlled the particle size of carbon nanodots via a combination of solvent, temperature and pH conditions and found a correlating decrease in optical gap of almost 1 eV as particle size increased from approximately 2 – 7 nm.[53]

Conjugated polymers made by metal catalysed cross coupling reactions are increasingly investigated as photocatalysts for hydrogen production with some examples being among the most active organic photocatalysts and only outperformed by highly optimised carbon nitride systems.[3] The advantage of these materials is the increased structural diversity that can be incorporated into monomers and a greater degree of control over the function groups present in polymer backbone. However, similarly to carbon nitride, these materials are frequently insoluble in common organic solvents and thus also have their microstructure – "fixed-in" during synthesis (Figure 3). One way around this is to conduct polymerisation reactions in mini-emulsion. In this case, growing polymer chains are confined within the droplets of oil in water-type emulsions which limits particle sizes compared to standard bulk precipitation polymerisation. This technique is compatible with a variety of different cross coupling reactions including Glaser, Sonogashira and Suzuki polymerisation,[54–57] meaning small polymer particles with a range of conjugated and aromatic backbone groups can be synthesised. This was recently used to synthesise 100 – 500 nm particles of linear and cross-linked polymer photocatalysts which outperformed their bulk analogues;[17] Under broad spectrum irradiation hydrogen evolution rates were 1.5 – 3 times higher which we attributed to the increased surface area of the emulsion derived samples compared to the bulk. Importantly the comparison between emulsion derived and precipitation polymerisation derived materials was conducted at the same photocatalyst concentration, meaning the mass normalised hydrogen evolution rates reflect an improvement in catalyst efficiency rather than improvements from moving out of the saturated regime of photocatalyst concentration, where 'excess' catalyst tends to reduce the mass normalised rate.[58] This can lead to significantly inflated hydrogen evolution rate (HER) for photocatalytic experiments conducted at low concentrations; For example, when the photocatalyst concentration of the most active material P10-e (Figure 4) was reduced from 0.1 to 0.013 mg mL^{-1} a similar amount of hydrogen (75%) was produced over 50 hours but the mass normalised hydrogen evolution rate increased from 14 to 60 mmol g^{-1} h^{-1}. Under optimised conditions P10-e displayed a very high EQE of 20% at 420 nm indicating emulsion derived materials can produce significant absolute amounts of hydrogen as well as displaying high mass normalised rates.

It should be noted that whilst the linear polymer P10-e showed good light absorption in the visible region, two conjugated microporous polymers made via emulsion polymerisation, S-CMP1-e and MeCMP-e, had significantly blue-shifted absorption onsets compared to their bulk analogues, suggesting the emulsion based synthesis may not be conducive to achieving high degrees of polymerisation.

The emulsion derived materials were tested using a number of different sacrificial electron donors which necessitated significantly different dispersant media. Interestingly the most active system – made up equal parts aqueous nanoparticles, MeOH and TEA – was made up of a mixture of 'free' nanoparticles and larger micro-scale aggregates. Other scavenger systems that did result in aggregation of the photocatalyst were found to have lower hydrogen evolution rates. Whether this was a particle size effect related to light scattering or was the result of different photocatalyst – sacrificial hole scavenger – dispersant interactions is unclear but these results indicate that reducing particle size / increasing catalysts active surface area is important, but not always the dominant factor determining a photocatalysts' activity.

Post-synthetic modification routes

In-synthesis routes allow for generating nanosized conjugated polymer nanoparticles directly but two-step approaches, whereby the semiconductor is first synthesised before processing it into nanoparticles, have also been extensively studied. For linear conjugated polymers typically a co-polymerisation of aromatic building blocks with monomers that bear alkyl side chains is performed to give polymers that are soluble in common organic solvents. These materials are then processed from solvents to give nanoparticles.

In 2016, Tian and co-workers used the soluble benzothiadiazole bearing PF8BT polymer (labelled PFBT in Figure 5), to make nanoparticles with very high mass normalised hydrogen evolution rates.[18] The solubility of PF8BT in THF means that a simple nanoprecipitation process could be employed to generate the nanoparticle photocatalysts, which were stabilised by an amphiphilic polystyrene/PEG co-polymer (PS-PEG- COOH). The initial HER of 8.3 mmol h^{-1} g^{-1} was found to be five orders of magnitude greater than the bulk F8BT polymer under the same conditions, though it is unclear if the bulk material can be evenly dispersed in the water/scavenger mixture. Despite the high HER a relatively low EQE of 0.7% at 420 nm was determined, which is most likely a result of insufficient light absorption due to the low concentration of the nanoparticles. For comparison a bulk benzothiadiazole/phenyl linear copolymer with micro-scale particles and measured at significantly higher concentrations was reported with an EQE of 4% at 420 nm, despite producing less than 1/3 of the mass normalised HER over visible wavelengths.[24] Interestingly, the nanoparticles (30-100 nm) undergo a degree of aggregation almost immediately when subjected to catalytic conditions (0.2 M ascorbic acid, $\lambda > 420$ nm) with an increase in average particle size of 20 nm within 5 minutes. This period seemed to correspond with the period before the maximum HER is reached. The authors suggest the two observations are related and that structural reorganisation to an active species is responsible for the delayed photocatalytic activity.

Following this pioneering publication several follow-up studies have been published on polymer nanoparticles made from solution processible polymer photocatalysts: The activity of benzothiadiazole/fluorene copolymer nanoparticles could be significantly increased by introducing thiophene units into the material (PFODTBT Figure 5).[19] This was rationalised by an increase in the light-absorption of the nanoparticles beyond 600 nm and resulted in a 500% increase in the mass

normalised HER to 63,000 μmol h^{-1} g^{-1}. Again, a relatively low EQE of close to 0.9% at 420 nm was reported although still reaches 0.6% at 550 nm as the absorption profile was extended further into the visible region. The thiophene bearing polymer also had more than twice the longevity compared to the original PF8BT material, but hydrogen evolution rates reduce over time and the material ceased to be active after just 4 hours. The authors cite aggregation as the reason for the fast deactivation of the photocatalyst although it is worthwhile noting that the bulk polymer shows a similar rate of deactivation. Others have not observed this deactivation for PF8BT nanoparticles,[13] which were instead found to give sustained hydrogen evolution over 20 hours, albeit with diethylamine as sacrificial hole scavenger and potentially differing light intensities.

In an attempt to further increase the surface area of PFODTBT dots were treated with ultrasonication resulting in hollow nanostructures.[59] Compared to solid nanoparticles a significant improvement in activity was reported and nanoparticles with varied Z-average diameters were fabricated by altering the polymer concentration in the fabrication process. Nanoparticles with a size of 50 nm were found to be more active with a sacrificial hydrogen evolution rate of 18,100 μmol h^{-1} g^{-1} compared to 4600 μmol h^{-1} g^{-1} and 2600 μmol h^{-1} g^{-1} for 70 and 90 nm sized nanoparticles of the same material (Figure 6). Experiments on PF8BT nanoparticles have found similar results to this study with the hydrogen evolution rate of particles with a Z-average of 50 nm more than twice that of particles with an Z-average of 90 nm.[33] HER varied less with particle size for batches with higher (> 100 nm) average particle sizes. Smaller particles were also found to have lower fluorescence intensity and shorter fluorescence lifetime than larger particles which was suggested to be due to the more efficient quenching of excitons by Pd in smaller nanoparticles; a result of the tendency of residual palladium to preferentially reside at the surface particles during the nanoprecipitation process.[33]

Previous studies have also investigated the effect of palladium content on the photocatalytic activity of PF8BT nanoparticles. The soluble nature of this polymer means it is possible to remove residual palladium from synthesis via preparative gel permeation chromatography. This allowed the authors to show convincingly that palladium does acts as a co-catalyst, as the PF8BT nanoparticle that were devoid of palladium was found to be inactive, whilst samples with loadings from 36 to 100 ppm resulted in an almost linear increase in activity with Pd content.[13] At higher levels a plateau was observed where an increase in palladium resulted in no further increase in activity. Despite similar particle sizes and palladium contents the mass normalised hydrogen evolution rate of these PF8BT nanoparticles was significantly lower than reported by Tian *et al.* (0.177 vs 8.3 mmol h^{-1} g^{-1}). It is possible that this is linked to the significantly higher nanoparticle concentration (0.13 vs 0.013 mg mL^{-1}) used for testing but the materials EQE was also less than 1/20th of the previously reported value which should, in theory, remove any concentration or set-up light intensity effects. These measurements use a different sacrificial electron donor (diethylamine) and a different stabilising copolymer, so these most likely contribute to this large variation in activity.

As opposed to adding metal nanoparticle co-catalysts, nanoparticles of PFTFQ (poly[(9,9'-dioctylfluorenyl-2,7-diyl)-co-(6,7-difluoro-2,3-bis(3-(hexyloxy)phenyl)-5,8-bis-(thiophen-2-yl)quinoxaline)]) were made with varied amounts of platinum complexes incorporated into the polymer's chemical structure (Figure 7).[60] After an optimisation 15 mol% of a platinum complex were found to give the highest activity of 11,200 μmol h^{-1} g^{-1}, with a modest EQE of 0.42%. The co-polymerisation of the complex was found to be more efficient than simply mixing the polymer with the complex during photocatalysis and taken together with other characterisation suggests that the platinum complex acts as the active site. A follow up study by the same authors explored a range of other potential building blocks and also studied the toxicity of these materials.[61] Iridium complexes have also been studied using a similar approach and incorporated into PFTBDD (poly[(9,9'-dioctylfluorenyl-2,7-diyl)-co-(2-thienyl-benzo [1,2-*c*:4,5-*c*']dithiophene-4,8-dione)]) resulting in 22-times higher activity for sacrificial hydrogen production compared to the co-polymer not containing the Ir-complex.[62]

Post-synthetic modification using precipitation techniques usually requires that the photocatalyst is soluble in an organic solvent. However, there are alternative methods for reducing particle size for insoluble bulk materials; Two dimensional materials such as covalent organic frameworks and triazine-based frameworks have potential to undergo exfoliation, which results in thin-layers that can also be nanosized and show enhanced photocatalytic activity.

In the context of conjugated photocatalysts this is probably most widely studied for carbon nitride materials.[63] Poly(triazine imide) can be exfoliated into nanosheets that are 1-2 nm high that have 18-times increased hydrogen evolution rates, though having a modest EQE of 1.3% at 400 nm due to low loadings (Figure 8).[64] Exfoliated tri-*s*-triazine based carbon nitrides have been reported following this with much a much higher EQE of 8.57% at 420 nm,[65] highlighting the potential of this approach in making nano-sized photocatalysts. Mixtures of bulk carbon nitride with exfoliated carbon nitride were found to be twice as active as bulk carbon nitride on its own with the latter thought to possess more catalytically active sites and be more exposed to the water/scavenger mixture.[66]

Covalent organic frameworks have also been shown to exfoliate,[25] however, so far no study has been reported that has studied size effects in detail. Materials such as aza-CMP, the condensation product of hexaketocyclohexane and 1,2,4,5-benzenetetramine, have been used as photocatalysts after exfoliation (Figure 9).[67] Significantly this photocatalyst is able to perform sacrificial water oxidation after loading with a cobalt co-catalyst due to the materials low (-6.08 V) HOMO energy level. Interestingly, the absorption on-set is far into the IR region at 1.22 eV allowing the material to produce oxygen even under NIR light illumination (λ > 800 nm). Another recent study focused on a conjugated microporous polymer comprised of tetra-substituted pyrene and bithiophene.[68]

When this photocatalyst was dispersed in different polar solvents it was found to enhance the photocatalytic activity for sacrificial hydrogen production significantly. This was ascribed to exfoliation of the material into nanosheets. A very high mass normalised rate of 303.7 mmol h^{-1} g^{-1} and very high EQEs (up to 6.9% close to the absorption maximum at 550 nm) were determined when the material was exfoliated in a water/*N*-methyl-2-pyrrolidone/ascorbic acid mixture.

Carbon dots can be synthesised by bottom up approaches, as described above, but reduced graphene oxide-based quantum dots and carbon nitride nanosheets can also be synthesised from bulk materials using Hummers-type methods, where oxidants, such as potassium permanganate or ferrate, are used to chemically exfoliate graphite[69] or carbon nitrides.[70] This route has been used to generate *N*-doped graphene oxide quantum dots that are reportedly capable of overall water splitting without any metal co-catalysts, albeit at very low rates. The stoichiometric ratio of hydrogen and oxygen produced by this system was not consistently 2:1 and unfortunately no EQE or solar-to-hydrogen conversion efficiency measurements were conducted so further investigation into these materials is desirable.[71]

Preparation of composites

The examples discussed so far are single semiconductor photocatalytic systems where charge separation mostly relies on electron transfer to a metal cocatalyst or scavenger molecule. However, charge separation can also be achieved by introducing a second semiconducting material to form a heterojunction,[72] with the interface providing the driving-force for exciton separation. This is a frequently used approach for change separation in blended polymer film solar cells[73] but if donor and acceptor type materials with suitable band structures are used this can also be applied to nanoparticle architectures for photocatalysis.

The first example of this strategy for hydrogen production used donor and acceptor type polymers generated by co-polymerising 9,9'di-*n*-octylfluorene with either triphenylamine or benzothiadiazole monomers.[74] Nanoprecipitation using THF solutions containing both the donor and acceptor polymers were then used to obtain blended nanoparticles containing both polymers. These had hydrogen evolution rates over five times higher than nanoparticles of either single polymer component. A physical mixture of the two single-component nanoparticles showed much smaller improvement compared to the blended nanoparticles indicating the polymer-polymer interface formed within nanoparticles was crucial to the improved photocatalytic activity, rather than inter-colloidal interaction. Photoluminescent behaviour of blended films of the donor and acceptor polymers was found to be consistent a with photoinduced charge transfer, suggesting that the heterojunction aids charge separation. When the triphenyl amine bearing donor polymer was replaced with PF8 (which has a lower HOMO energy), or an acceptor polymer with a raised HOMO energy was used, then photoluminescent behaviour of polymer blends switches to FRET characteristics and negligible improvements in the observed hydrogen evolution rates were observed in the blended nanoparticles. This suggests that a large offset in band energy between polymers is required to facilitate charge separation. In this system, both HER and the improvement on moving from mixtures to the blended particles was found to reduce somewhat as the donor/acceptor ratio was changed from 1:1 to 4:1.

Another recent study used a high-throughput approach and screened a library of 237 2-componant blended nanoparticles consisting of 1 of 4 donor type and 1 of 5 acceptor type polymers combined, via nanoprecipitation, in various weight ratios.[75] In nearly all cases blended nanoparticles outperformed their single component analogues. The most active blend consisted of PCDTBT donor with a $PC_{60}BM$ acceptor in a 3:7 ratio which had a very high mass normalised HER of 105 mmol g^{-1} h^{-1} under visible light. Despite being tested at a relatively low concentration of 46 μg mL^{-1} these particles also showed a significant EQE of 3.0% at 595 nm. Notably a non-fullerene acceptor, ITIC-2F, also showed very high activity combined with PCDTBT at the same 3:7 optimal polymer ratio. The fullerene and non-fullerene containing blends outperformed physical mixtures of single component nanoparticles by 23 and 18 times respectively, again indicating heterojunction formation within nanostructures aids photocatalysis.

Recently Kosco *et al.* generated blended nanoparticles of PTB7-Th donor and the non-fullerene acceptor polymer, EH-IDTBR (Figure 10).[76] In this case, HERs of the blended materials were between 1 and 2 orders of magnitude higher than physical nanoparticle mixtures. These particles were precipitated from a chloroform-water mini-emulsion, rather than miscible water–THF solutions and the morphology of the resultant particle blends showed a strong dependence on the surfactant used to stabilise the emulsion. SDS – a long alkyl chain bearing amphiphile – appeared to show stronger affiliation for the PTB7-Th donor polymer resulting in its accumulation at the surface of the micelle and the formation of a EH-IDTBR / PTB7-TH core/shell structure, while a thiophene-based surfactant (TEBs) produced a more intermixed morphology. This structural difference was accompanied by an order of magnitude increase in HER, suggesting the highly interpenetrated domains of donor and acceptor polymers present in the TEBs nanoparticles leads to more effective charge separation and/or the presence of both polymers at the nanoparticle surface enables the extraction of both holes (by SED) and electrons (by Pt cocatalyst). Experiments varying the ratio of donor to acceptor polymer found that whilst the TEBs nanoparticles performed best at a donor/acceptor ratio of 3:7 (28.1 mmol g^{-1} h^{-1}) the SDS nanoparticles required 90% EH-IDTBR to give optimal performance (3.0, mmol g^{-1} h^{-1}), likely due to the inability of PTB7-TH to fully encapsulate the acceptor polymer at this ratio. With optimal co-catalyst loading the TEBs nanoparticles showed an average HER of 64.4 mmol g^{-1} h^{-1} over 16 hours of irradiation and high EQEs of up to 6.2% at 700 nm.

Interestingly, the activity of the single component polymer nanoparticles and a physical mixture of the two types of polymer nanoparticles also show increases in HER upon

moving from SDS to TEBs.[76] In other studies it has been found that adding surfactant to the nanoprecipitation process is actually detrimental to the activity of the resultant catalysts.[75] These results indicate that the choice of surfactant used to stabilise nanoparticle photocatalysts may influence more than just the polymer-polymer interface, this is certainly an area that warrants further study.

Polymer nanoparticles have also been combined with carbon nitride nanosheets to form heterojunctions.[77] Using a PIFDTBT polymer significantly extends the light absorption into the visible region of the composite and the interface also seems to increase the charge-separation efficiency, just as in the nanoparticle heterojunctions as evident from electrochemical measurements. A maximum hydrogen evolution rate of 578.1 $\mu mol\ h^{-1}\ g^{-1}$ with an EQE of 3.4% at 420 nm was determined while the individual components were found to be inactive.

Nanoscale heterojunctions can also be obtained by combining 2D conjugated organic polymers not bearing solubilising side chains. Nanosheets with an approximate thickness of 4 nm of a C_2N donor polymer and aza-CMP acceptor polymer were used to generate a polymer-polymer Van der Waals heterostructure.[78] X-Ray absorption near-edge structure spectroscopy indicated π-π stacking interactions between the two types of polymer sheet and photocurrent measurements also showed a higher photocurrent for the heterostructure compared to the individual materials. Remarkably, this heterostructure was reported to evolve stochiometric hydrogen and oxygen from pure water under visible light, without the addition of any metal cocatalysts, with a solar-to-hydrogen efficiency of 0.23%. This value could be increased to 0.73% with the addition of a reduced graphene oxide as a solid electron mediator and appropriate Co and Pt cocatalysts. More work on these exciting nanostructures is needed though to fully explore their potential for future application.

Conclusions and outlook

Over the last 5 years it has become clear that conjugated polymer photocatalysts have potential to be highly efficient photocatalysts for water splitting. In terms of sacrificial hydrogen production, their performance is rapidly approaching levels of activity previously only observed for inorganic semiconductors.

Several factors that have a significant effect on the photocatalytic performance of conjugated material photocatalysts have been identified and studied. Among them particle size is found to be an important factor and has been frequently shown to have a large impact on the performance of photocatalysts. This can be explained by the fact that excitons have limited diffusion lengths, resulting in recombination of those excitons that are generated within particles at positions beyond a few tens of nanometres. Several publications have exploited this and made nanosized materials that are orders of magnitude more active than bulk photocatalysts. Despite this, particle size is frequently not considered when looking at bulk materials. We argue that as this is an important factor in understanding materials' performance and should therefore be studied for all materials, particularly in cases with small differences in activity between photocatalysts.

Another important factor that requires attention are the measurements themselves. Standardisation of performance evaluation is desirable for all photocatalytic systems, but the polymer photocatalyst community in particular appears to include a wide range of different set-ups and conditions, making activity comparisons very challenging. Often headline rates are expressed as micro- or millimole of hydrogen per hour and normalised to weight (typically per gram), but the absolute amounts of hydrogen produced are a far more important quantity and should be reported alongside the rates. Considering gas evolution rates are highly depended on the set-up, pressure of operation and light intensity, direct comparisons are effectively meaningless. It is therefore important that quantum efficiencies are also reported as these allow for better comparison of the results across different laboratories, but here also concentration effects have to be taking into account (Figure 11).

Normalised rates also mask another issue when using nanoparticle systems: Often the loadings are very low, meaning that the absolute amounts of hydrogen produced are very small when compared to mass normalised rates. For nanoparticle systems to become a useful technology studies should aim to increase photocatalyst concentration so as to produce significant (absolute) amounts of hydrogen for a given area of illumination. If this is achieved then another factor to consider is that of synthetic scale-up; aside from hydrothermal synthesis of carbon dots, the synthesis methods described in this article mostly yield very small amounts of photocatalysts. Routes to producing nanostructured materials on gram or kilogram scale will have to be explored for the field to make further progress.

Hydrogen production will ultimately have to be coupled to water oxidation, either using a single component system or, more likely, using a paired Z-scheme of two semiconductors. Nanocomposites could play an important role in this latter type of system as they allow for excellent contact with between two catalyst systems, such as a metal oxide and a polymer, that can drive water oxidation and proton reduction, respectively. Nanoparticles would be suited to Z-scheme systems that rely on colloidal interactions between semiconductors[79] as well as those that use solution based redox shuttles[80] or deposit semiconductor particles on solid electron mediator sheet structures.[7]

Another crucial aspect that needs improving for nanoparticle systems is their longer-term stability. Some reports show deactivation of the catalysis occurs after only a few hours, and faster than bulk materials. It is unclear if this is due to underlying stability issues which could also be exacerbated by the low concentrations of nanoparticles often used - thus deactivation is not masked by the large amounts of photocatalyst typically present in bulk experiments - or other effects such as aggregation play a role. Control over aggregation will also be crucial in the future, with colloidal

stability being possibly an even bigger challenge if moving towards systems that use seawater. This is could be archived by immobilising of photocatalyst nanoparticles onto surfaces using functional groups such as amines[81] or embedding into matrices.

Overall, conjugated nanoparticular photocatalysts have shown significant potential and are set to play an important role for photocatalytic water splitting in the future. Composites are particularly exciting in this respect, and interfaces with biology, such as enzymes offer further potential directions.[82] Beyond this there are many other photocatalytic applications that have not yet been studied with conjugated nanomaterial photocatalysts such as CO_2 reduction, hydrogen peroxide production and nitrogen fixation, and it can be expected that conjugated nanoparticular photocatalysts will be applied to these areas soon too.

Conflicts of interest

There are no conflicts to declare

Acknowledgements

R.S.S thanks the University of Strathclyde for financial support through The Strathclyde Chancellor's Fellowship Scheme.

Notes and references

1 J. H. Kim, D. Hansora, P. Sharma, J.-W. Jang and J. S. Lee, *Chem. Soc. Rev.*, 2019, **48**, 1908–1971.

2 L. Yao, A. Rahmanudin, N. Guijarro and K. Sivula, *Adv. Energy Mater.*, 2018, **8**, 1802585.

3 Y. Wang, A. Vogel, M. Sachs, R. S. Sprick, L. Wilbraham, S. J. A. Moniz, R. Godin, M. A. Zwijnenburg, J. R. Durrant, A. I. Cooper and J. Tang, *Nat. Energy*, 2019, **4**, 746–760.

4 J. Jayakumar and H. Chou, *ChemCatChem*, 2020, **12**, 689–704.

5 C. Zhao, Z. Chen, R. Shi, X. Yang and T. Zhang, *Adv. Mater.*, 2020, **32**, 1907296.

6 T. G. Pinaud Blaise A, Benck Jesse D, Seitz Linsey C, Forman Arnold J, Chen Zhebo, Deutsch, B. D. James, K. N. Baum, G. N. Baum, S. Ardo, H. Wang and T. F. Jaramillo, *Energy Environ. Sci.*, 2013, **6**, 1983–2002.

7 Q. Wang, T. Hisatomi, Q. Jia, H. Tokudome, M. Zhong, C. Wang, Z. Pan, T. Takata, M. Nakabayashi, N. Shibata, Y. Li, I. D. Sharp, A. Kudo, T. Yamada and K. Domen, *Nat. Mater.*, 2016, **15**, 611–615.

8 T. Takata, J. Jiang, Y. Sakata, M. Nakabayashi, N. Shibata, V. Nandal, K. Seki, T. Hisatomi and K. Domen, *Nature*, 2020, **581**, 411–414.

9 X. Wang, K. Maeda, A. Thomas, K. Takanabe, G. Xin, J. M. Carlsson, K. Domen and M. Antonietti, *Nat. Mater.*, 2009, **8**, 76–80.

10 S. Yanagida, A. Kabumoto, K. Mizumoto, C. Pac and K. Yoshino, *J. Chem. Soc. Chem. Commun.*, 1985, 474–475.

11 R. S. Sprick, B. Bonillo, R. Clowes, P. Guiglion, N. J. Brownbill, B. J. Slater, F. Blanc, M. A. Zwijnenburg, D. J. Adams and A. I. Cooper, *Angew. Chem. Int. Ed.*, 2016, **55**, 1792–1796.

12 M. Sachs, R. S. Sprick, D. Pearce, S. A. J. Hillman, A. Monti, A. A. Y. Guilbert, N. J. Brownbill, S. Dimitrov, X. Shi, F. Blanc, M. A. Zwijnenburg, J. Nelson, J. R. Durrant and A. I. Cooper, *Nat. Commun.*, 2018, **9**, 4968.

13 J. Kosco, M. Sachs, R. Godin, M. Kirkus, L. Francas, M. Bidwell, M. Qureshi, D. Anjum, J. R. Durrant and I. McCulloch, *Adv. Energy Mater.*, 2018, **8**, 1802181.

14 R. S. Sprick, L. Wilbraham, Y. Bai, P. Guiglion, A. Monti, R. Clowes, A. I. Cooper and M. A. Zwijnenburg, *Chem. Mater.*, 2018, **30**, 5733–5742.

15 Z. Hu, X. Zhang, Q. Yin, X. Liu, X. Jiang, Z. Chen, X. Yang, F. Huang and Y. Cao, *Nano Energy*, 2019, **60**, 775–783.

16 D. J. Woods, S. A. J. Hillman, D. Pearce, L. Wilbraham, L. Q. Flagg, W. Duffy, I. McCulloch, J. R. Durrant, A. A. Y. Guilbert, M. A. Zwijnenburg, R. S. Sprick, J. Nelson and A. I. Cooper, *Energy Environ. Sci.*, 2020, **13**, 1843–1855.

17 C. M. Aitchison, R. S. Sprick and A. I. Cooper, *J. Mater. Chem. A*, 2019, **7**, 2490–2496.

18 L. Wang, R. Fernández-Terán, L. Zhang, D. L. A. Fernandes, L. Tian, H. Chen and H. Tian, *Angew. Chem. Int. Ed.*, 2016, **55**, 12306–12310.

19 P. B. Pati, G. Damas, L. Tian, D. L. A. Fernandes, L. Zhang, I. B. Pehlivan, T. Edvinsson, C. M. Araujo and H. Tian, *Energy Environ. Sci.*, 2017, **10**, 1372–1376.

20 R. S. Sprick, J. X. Jiang, B. Bonillo, S. Ren, T. Ratvijitvech, P. Guiglion, M. A. Zwijnenburg, D. J. Adams and A. I. Cooper, *J. Am. Chem. Soc.*, 2015, **137**, 3265–3270.

21 D. Schwarz, A. Acharjya, A. Ichangi, Y. S. Kochergin, P. Lyu, M. V. Opanasenko, J. Tarábek, J. Vacek Chocholoušová, J. Vacek, J. Schmidt, J. Čejka, P. Nachtigall, A. Thomas and M. J. Bojdys, *ChemSusChem*, 2019, **12**, 194–199.

22 Y. Bai, D. J. Woods, L. Wilbraham, C. M. Aitchison, M. A. Zwijnenburg, R. S. Sprick and A. I. Cooper, *J. Mater. Chem. A*, 2020, **8**, 8700–8705.

23 R. S. Sprick, Y. Bai, A. A. Y. Guilbert, M. Zbiri, C. M. Aitchison, L. Wilbraham, Y. Yan, D. J. Woods, M. A. Zwijnenburg and A. I. Cooper, *Chem. Mater.*, 2019, **31**, 305–313.

24 C. Yang, B. C. Ma, L. Zhang, S. Lin, S. Ghasimi, K. Landfester, K. A. I. Zhang and X. Wang, *Angew. Chem. Int. Ed.*, 2016, **55**, 9202–9206.

25 X. Wang, L. Chen, S. Y. Chong, M. A. Little, Y. Wu, W.-H. Zhu, R. Clowes, Y. Yan, M. A. Zwijnenburg, R. S. Sprick and A. I. Cooper, *Nat. Chem.*, 2018, **10**, 1180–1189.

26 R. K. Sharma, P. Yadav, M. Yadav, R. Gupta, P. Rana, A. Srivastava, R. Zbořil, R. S. Varma, M. Antonietti and M. B. Gawande, *Mater. Horizons*, 2020, **7**, 411–454.

27 C. M. Aitchison, M. Sachs, M. A. Little, L. Wilbraham, N. J. Brownbill, C. M. Kane, F. Blanc, M. A. Zwijnenburg, J. R. Durrant, R. S. Sprick and A. I. Cooper, *Chem. Sci.*, 2020, **11**, 8744–8756.

28 X. Yang, Z. Hu, Q. Yin, C. Shu, X. X. F. Jiang, J. Zhang, X. Wang, J. X. Jiang, F. Huang, Y. Cao, Q. Yin, Y. Cao, C. Shu, X. Wang, F. Huang, X. Yang, Z. Hu, X. X. F. Jiang, Q. Yin, C. Shu,

X. X. F. Jiang, J. Zhang, X. Wang, J. X. Jiang, F. Huang and Y. Cao, *Adv. Funct. Mater.*, 2019, **29**, 1–9.

29 V. W. H. Lau, M. B. Mesch, V. Duppel, V. Blum, J. Senker and B. V. Lotsch, *J. Am. Chem. Soc.*, 2015, **137**, 1064–1072.

30 C. M. Aitchison, C. M. Kane, D. P. McMahon, P. R. Spackman, A. Pulido, X. Wang, L. Wilbraham, L. Chen, R. Clowes, M. A. Zwijnenburg, R. S. Sprick, M. A. Little, G. M. Day and A. I. Cooper, *J. Mater. Chem. A*, 2020, **8**, 7158–7170.

31 J. Byun and K. A. I. Zhang, *Mater. Horizons*, 2020, **7**, 15–31.

32 H. Wang, S. Jin, X. Zhang and Y. Xie, *Angew. Chem. Int. Ed.*, 2020, DOI: 10.1002/ange.202002241.

33 M. Sachs, H. Cha, J. Kosco, C. M. Aitchison, L. Francàs, S. Corby, C.-L. Chiang, A. A. Wilson, R. Godin, A. Fahey-Williams, A. I. Cooper, R. S. Sprick, I. McCulloch and J. R. Durrant, *J. Am. Chem. Soc.*, 2020, **142**, 14574–14587.

34 R. S. Sprick, Z. Chen, A. J. Cowan, Y. Bai, C. M. Aitchison, Y. Fang, M. A. Zwijnenburg, A. I. Cooper and X. Wang, *Angew. Chem. Int. Ed.*, 2020, **132**, 18854–18859.

35 H. Najafov, B. Lee, Q. Zhou, L. C. Feldman and V. Podzorov, *Nat. Mater.*, 2010, **9**, 938–943.

36 G. Zhang, G. Li, Z.-A. A. Lan, L. Lin, A. Savateev, T. Heil, S. Zafeiratos, X. Wang and M. Antonietti, *Angew. Chem. Int. Ed.*, 2017, **129**, 13445–13449.

37 G. Zhang, L. Lin, G. Li, Y. Zhang, A. Savateev, S. Zafeiratos, X. Wang and M. Antonietti, *Angew. Chem. Int. Ed.*, 2018, **57**, 9372–9376.

38 D. J. Martin, K. Qiu, S. A. Shevlin, A. D. Handoko, X. Chen, Z. Guo and J. Tang, *Angew. Chem. Int. Ed.*, 2014, **53**, 9240–9245.

39 Y. Jun, J. Park, S. U. Lee, A. Thomas, W. H. Hong and G. D. Stucky, 2013, 11289–11293.

40 Y. S. Jun, E. Z. Lee, X. Wang, W. H. Hong, G. D. Stucky and A. Thomas, *Adv. Funct. Mater.*, 2013, **23**, 3661–3667.

41 M. Shalom, S. Inal, C. Fettkenhauer, D. Neher and M. Antonietti, *J. Am. Chem. Soc.*, 2013, **135**, 7118–7121.

42 W. Che, W. Cheng, T. Yao, F. Tang, W. Liu, H. Su, Y. Huang, Q. Liu, J. Liu, F. Hu, Z. Pan, Z. Sun and S. Wei, *J. Am. Chem. Soc.*, 2017, **139**, 3021–3026.

43 K. Maeda, X. Wang, Y. Nishihara, D. Lu, M. Antonietti and K. Domen, *J. Phys. Chem. C*, 2009, **113**, 4940–4947.

44 H. Luo, Q. Guo, P. Á. Szilágyi, A. B. Jorge and M. M. Titirici, *Trends Chem.*, 2020, **2**, 623–637.

45 L. Cao, S. Sahu, P. Anilkumar, C. E. Bunker, J. Xu, K. A. S. Fernando, P. Wang, E. A. Guliants, K. N. Tackett and Y.-P. Sun, *J. Am. Chem. Soc*, 2011, **133**, 4754–4757.

46 B. C. M. Martindale, G. A. M. Hutton, C. A. Caputo and E. Reisner, *J. Am. Chem. Soc.*, 2015, **137**, 6018–6025.

47 B. C. M. Martindale, E. Joliat, C. Bachmann, R. Alberto and E. Reisner, *Angew. Chem. Int. Ed.*, 2016, **55**, 9402–9406.

48 D. S. Achilleos, W. Yang, H. Kasap, A. Savateev, Y. Markushyna, J. R. Durrant and E. Reisner, *Angew. Chem. Int. Ed.*, 2020, **59**, 18184–18188.

49 A. B. Bourlinos, A. Stassinopoulos, D. Anglos, R. Zboril, M. Karakassides and E. P. Giannelis, *Small*, 2008, **4**, 455–458.

50 Z. C. Yang, M. Wang, A. M. Yong, S. Y. Wong, X. H. Zhang, H. Tan, A. Y. Chang, X. Li and J. Wang, *Chem. Commun.*, 2011, **47**, 11615–11617.

51 S. Y. Park, H. U. Lee, E. S. Park, S. C. Lee, J. W. Lee, S. W. Jeong, C. H. Kim, Y. C. Lee, Y. S. Huh and J. Lee, *ACS Appl. Mater. Interfaces*, 2014, **6**, 3365–3370.

52 J. T. Margraf, V. Strauss, D. M. Guldi and T. Clark, *J. Phys. Chem. B*, 2015, **119**, 7258–7265.

53 F. Yuan, Z. Wang, X. Li, Y. Li, Z. Tan, L. Fan and S. Yang, *Adv. Mater.*, 2017, **29**, 1604436.

54 M. C. Baier, J. Huber and S. Mecking, *J. Am. Chem. Soc.*, 2009, **131**, 14267–14273.

55 K. Wu, J. Guo and C. Wang, *Chem. Commun.*, 2014, **50**, 695–697.

56 B. C. Ma, S. Ghasimi, K. Landfester, F. Vilela and K. A. I. Zhang, *J. Mater. Chem. A*, 2015, **3**, 16064–16071.

57 E. Hittinger, A. Kokil and C. Weder, *Angew. Chem. Int. Ed.*, 2004, **43**, 1808–1811.

58 H. Kisch, *Angew. Chemie - Int. Ed.*, 2010, **49**, 9588–9589.

59 A. Liu, C.-W. Tai, K. Holà and H. Tian, *J. Mater. Chem. A*, 2019, 4797–4803.

60 P.-J. Tseng, C.-L. Chang, Y.-H. Chan, L.-Y. Ting, P.-Y. Chen, C.-H. Liao, M.-L. Tsai and H.-H. Chou, *ACS Catal.*, 2018, **8**, 7766–7772.

61 C.-L. Chang, W.-C. Lin, C.-Y. Jia, L.-Y. Ting, J. Jayakumar, M. H. Elsayed, Y.-Q. Yang, Y.-H. Chan, W.-S. Wang, C.-Y. Lu, P.-Y. Chen and H.-H. Chou, *Appl. Catal. B Environ.*, 2020, **268**, 118436.

62 W.-C. Lin, M. H. Elsayed, J. Jayakumar, L.-Y. Ting, C.-L. Chang, A. M. Elewa, W.-S. Wang, C.-C. Chung, C.-Y. Lu and H.-H. Chou, *Int. J. Hydrogen Energy*, 2020, **56**, 32072-32081.

63 L. Lin, Z. Yu and X. Wang, *Angew. Chem. Int. Ed.*, 2019, **58**, 6164–6175.

64 K. Schwinghammer, M. B. Mesch, V. Duppel, C. Ziegler, J. Senker and B. V. Lotsch, *J. Am. Chem. Soc.*, 2014, **136**, 1730–1733.

65 H. Ou, L. Lin, Y. Zheng, P. Yang, Y. Fang and X. Wang, *Adv. Mater.*, 2017, **29**, 1700008.

66 K. L. Corp and C. W. Schlenker, *J. Am. Chem. Soc.*, 2017, **139**, 7904–7912.

67 L. Wang, Y. Wan, Y. Ding, Y. Niu, Y. Xiong, X. Wu and H. Xu, *Nanoscale*, 2017, **9**, 4090–4096.

68 J. Z. Cheng, L. L. Liu, G. Liao, Z. Q. Shen, Z. R. Tan, Y. Q. Xing, X. X. Li, K. Yang, L. Chen and S. Y. Liu, *J. Mater. Chem. A*, 2020, **8**, 5890–5899.

69 H. Yu, B. Zhang, C. Bulin, R. Li and R. Xing, *Sci. Rep.*, 2016, **6**, 1–7.

70 J. Xu, L. Zhang, R. Shi and Y. Zhu, *J. Mater. Chem. A*, 2013, **1**, 14766–14772.

71 T. F. Yeh, C. Y. Teng, S. J. Chen and H. Teng, *Adv. Mater.*, 2014, **26**, 3297–3303.

72 H. Yang, H. Amari, L. Liu, C. Zhao, H. Gao, A. He, N. Browning, M. A. Little, R. S. Sprick and A. Cooper, *Nanoscale*, 2020, DOI:10.1039/D0NR05801G.

73 T. Ameri, P. Khoram, J. Min and C. J. Brabec, *Adv. Mater.*, 2013, **25**, 4245–4266.

74 J. Wang, Y. Shen, Y. Li, S. Liu and Y. Zhang, *Chem. Eur. J.*, 2016, **22**, 12449–12454.

75 H. Yang, X. Li, R. S. Sprick and A. I. Cooper, *Chem. Commun.*, 2020, **56**, 6790–6793.

76 J. Kosco, M. Bidwell, H. Cha, T. Martin, C. T. Howells, M. Sachs, D. H. Anjum, S. Gonzalez Lopez, L. Zou, A. Wadsworth, W. Zhang, L. Zhang, J. Tellam, R. Sougrat, F. Laquai, D. M. DeLongchamp, J. R. Durrant and I. McCulloch, *Nat. Mater.*, 2020, **19**, 559–565.

77 W. Zhou, T. Jia, D. Zhang, Z. Zheng, W. Hong and X. Chen, *Appl. Catal. B Environ.*, 2019, **259**, 118067.

78 L. Wang, X. Zheng, L. Chen, Y. Xiong and H. Xu, *Angew. Chem. Int. Ed.*, 2018, **57**, 3454–3458.

79 A. Kudo, S. Yoshino, T. Tsuchiya, Y. Udagawa, Y. Takahashi, M. Yamaguchi, I. Ogasawara, H. Matsumoto and A. Iwase, *Faraday Discuss.*, 2019, **215**, 313–328.

80 Y. Qi, Y. Zhao, Y. Gao, D. Li, Z. Li, F. Zhang and C. Li, *Joule*, 2018, **2**, 2393–2402.

81 K. L. Materna, N. Lalaoui, J. A. Laureanti, A. P. Walsh, B. P. Rimgard, R. Lomoth, A. Thapper, S. Ott, W. J. Shaw, H. Tian and L. Hammarström, *ACS Appl. Mater. Interfaces*, 2020, **12**, 4501–4509.

82 K. Holá, M. V. Pavliuk, B. Németh, P. Huang, L. Zdražil, H. Land, G. Berggren and H. Tian, *ACS Catal.*, 2020, **10**, 9943–9952.

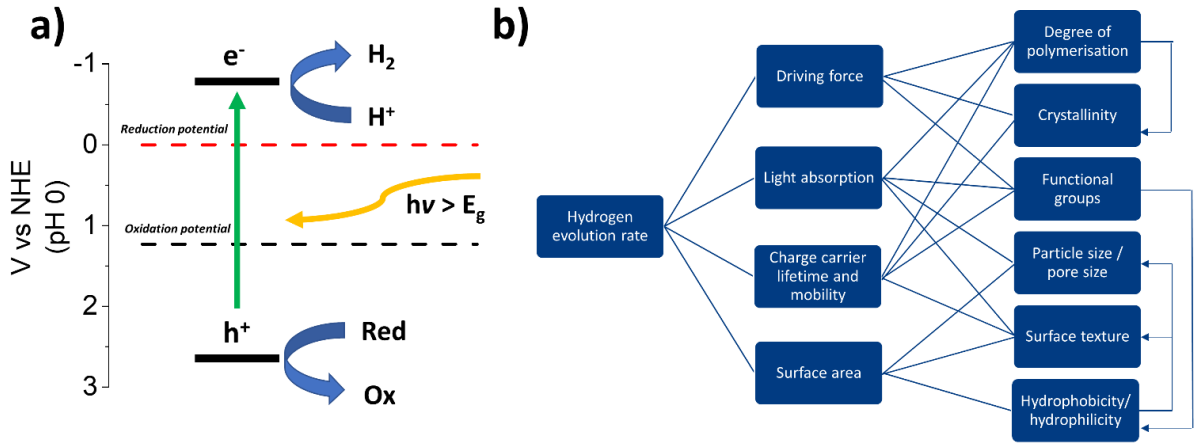

Figure 1. a) Mechanism of photocatalytic hydrogen production; b) Factors that affect the photocatalytic performance of polymer photocatalysts.

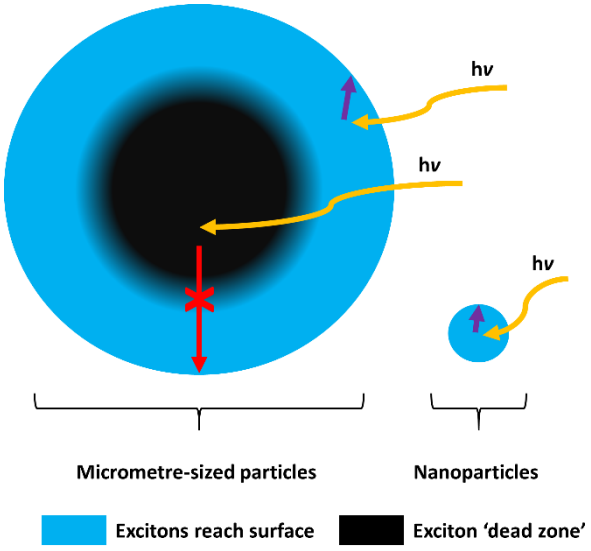

Figure 2. Different particle sizes and 'dead zone' within these particles.

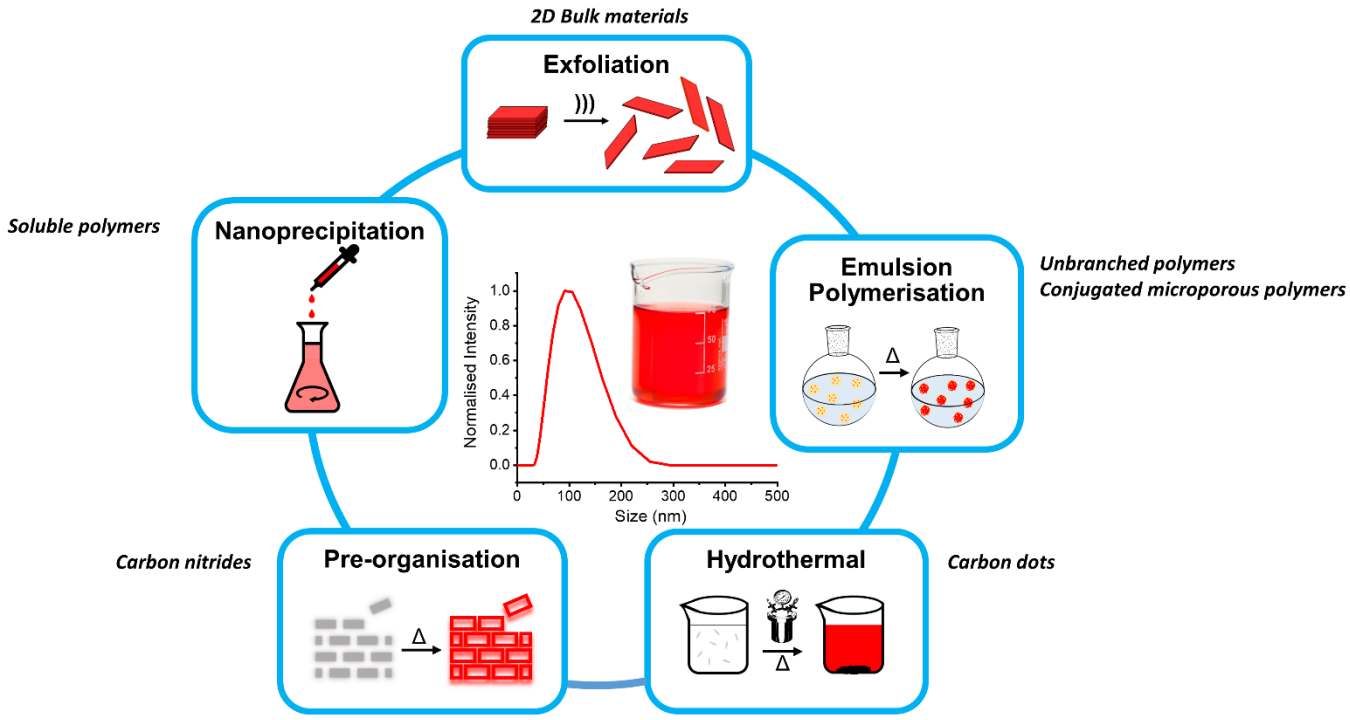

Figure 3. Methods of nanoparticle fabrication and example material classes that can be accessed. **Exfoliation:** 2D Nanosheets are generated by applying mechanical shear stress to suspensions of bulk material or by reaction with chemical exfoliators such as oxidants. **Emulsion Polymerisation:** Polymerisation reactions are performed within droplets of an emulsion that limit their particle size. **Hydrothermal:** Small molecule organic precursors are reacted in water at high temperature and pressure and nanoparticle products isolated. **Pre-organisation:** Crystalline precursors are used for the synthesis or carbon nitride type materials. **Nanoprecipitation:** Dilute polymer solutions are added to a miscible secondary solvent that induces precipitation of the polymer.

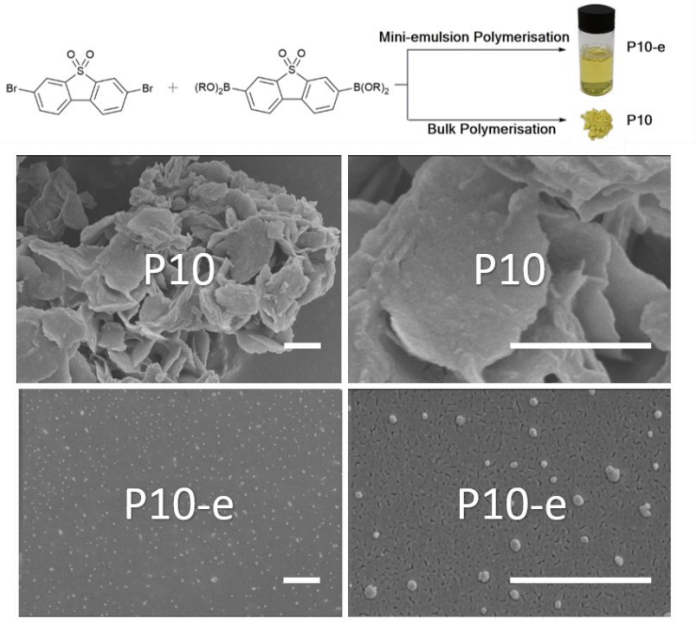

Figure 4. Top: Chemical structures and bottom: SEM images of bulk and emulsion derived polymers P10 and P10-e (Scale bars are 1 µm). Adapted from Ref. [17] with permission from the Royal Society of Chemistry.

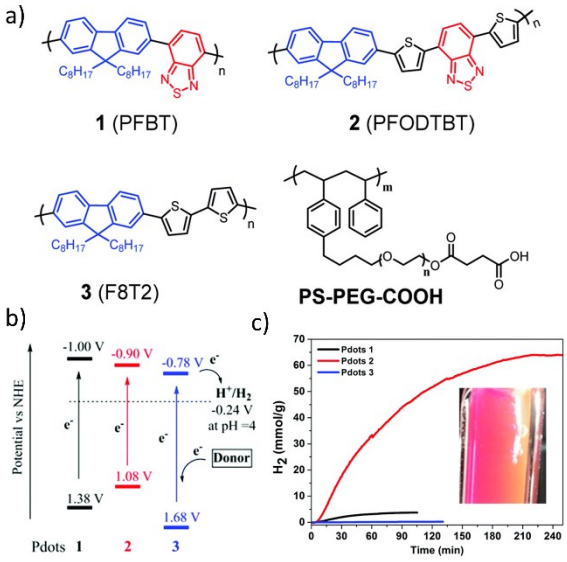

Figure 5. a) Structures of polymers 1-3 and amphiphilic PS-PEG- COOH polymer; b) Band positions of polymers 1-3; c) Sacrificial hydrogen evolution from water of polymer nanoparticles of polymers 1-3. Reproduced from Ref. [59] with permission from the Royal Society of Chemistry.

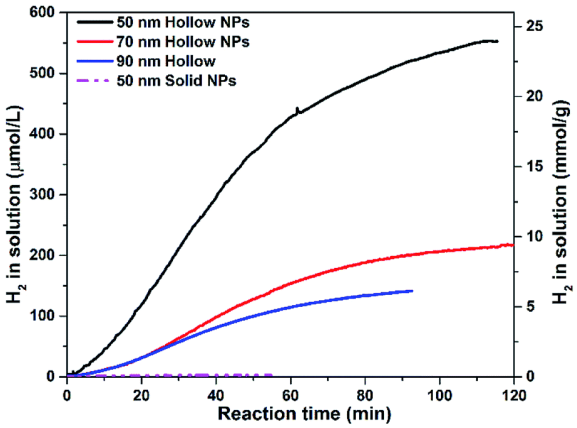

Figure 6. Effect of the particle size on the sacrificial hydrogen evolution from water under visible light irradiation of hollow polymer nanoparticles of polymers 2. Reproduced from Ref. [19] with permission from the Royal Society of Chemistry.

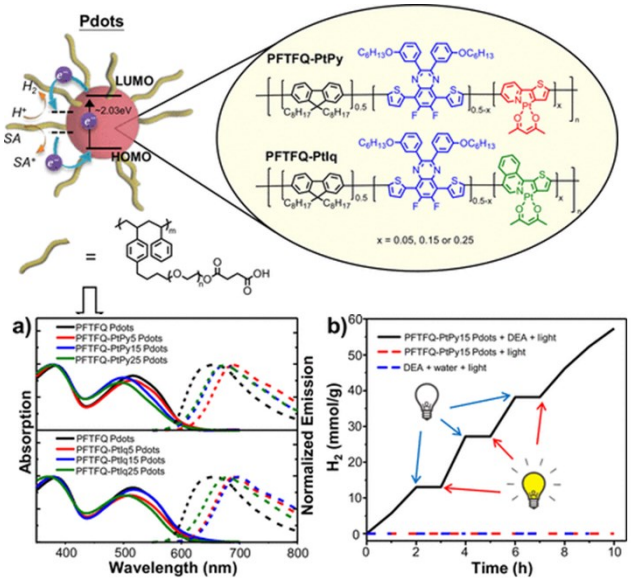

Figure 7. Top: Structures of cycloplatinated polymer dots; a) UV-Vis and photoluminescence spectra; b) Sacrificial hydrogen evolution from water under visible light irradiation. Adapted with permission from[60]. Copyright 2018 American Chemical Society.

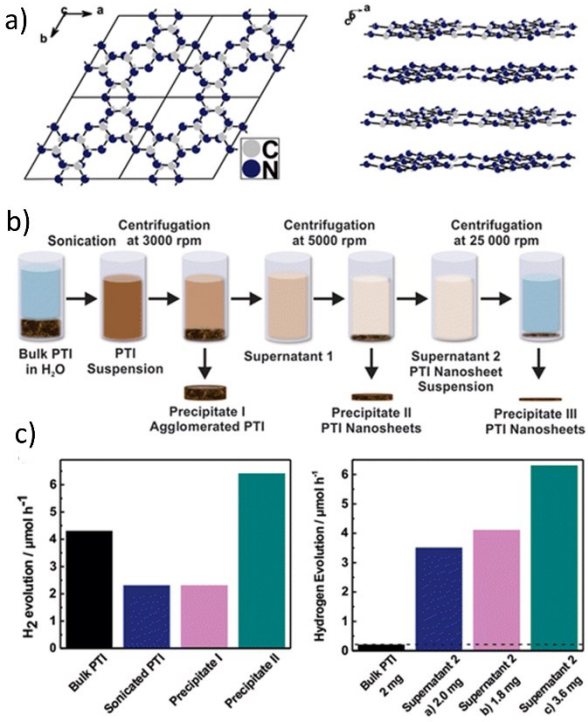

Figure 8. a) Idealised poly(triazine imide) (PTI) structure; b) exfoliation procedure; c) Sacrificial hydrogen evolution from water under visible light irradiation of bulk PTI and nanosheet suspensions. Adapted with permission from [64]. Copyright 2014 American Chemical Society.

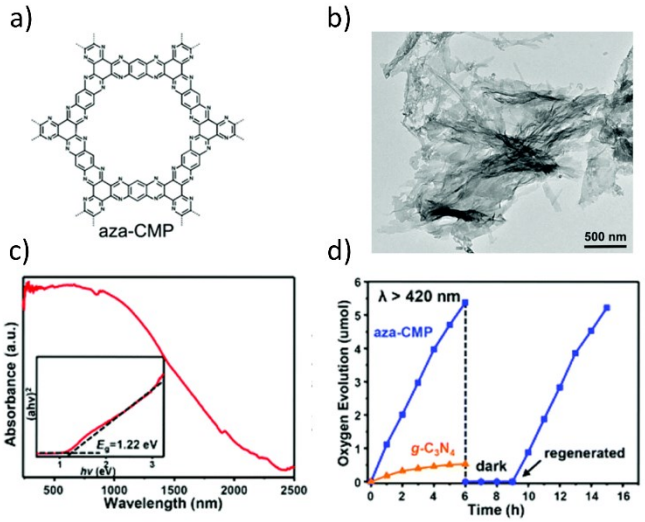

Figure 9. Idealised structure of aza-CMP; b) TEM Image of liquid-exfoliated aza-CMP nanosheets; c) UV-Vis diffuse reflectance spectrum of aza-CMP nanosheets; d) Sacrificial oxygen evolution from water of aza-CMP nanosheets under visible light irradiation. Adapted from Ref. [67] with permission from the Royal Society of Chemistry.

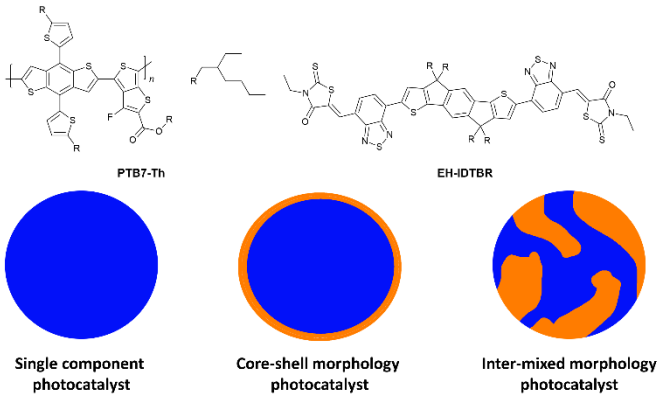

Figure 10. Top: Structures of PTB7-TH and EH-IDTBR. Bottom: Different morphologies of polymer nanoparticles reported in reference.[76]

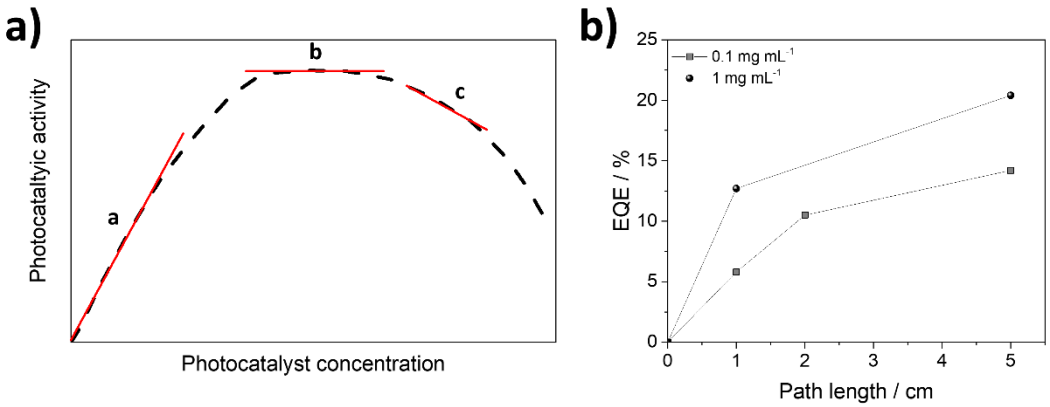

Figure 11. a) Dependence of the photocatalytic activity on the photocatalyst concentration[58] (a, linear regime; b, plateau region; c, region of decrease due to increased scattering); b) External quantum efficiencies of P10-e for sacrificial hydrogen evolution from water measured at different concentrations and with different path lengths (data taken from reference [17]).